
Boosting Inference with Guided Reasoning: Stochastic Exploration for Recursive Models

Andrew Corbett^{*1} Archit Sood^{*1} Anna Tzatzopoulou^{*1} Sai-Aakash Ramesh¹ Tim Dodwell^{1,2}

Abstract

Recent work on recursive architectures has shown that tiny neural networks can be surprisingly powerful on structured reasoning tasks. The trick is to model reasoning trajectories with a latent dynamical system. We argue that the inference-time behaviour of these architectures is best understood as approximate inference over latent reasoning trajectories, with deterministic recursion as the one-particle, zero-noise limit. We make this view operational through *guided stochastic exploration*: stochastic perturbations of the reasoning dynamics propose neighbouring trajectories, and the model’s existing early-stopping head reweights them online. The framework yields three label-free diagnostics: local stability, guide alignment, and cloud-token entropy. These predict, from inference traces alone, whether the procedure will help and which of its outputs to trust. On Sudoku-Extreme it lifts exact-solve accuracy from 85.9% to 98.0% without retraining; on Maze-Hard the diagnostics flag a misaligned guide, as validation performance later confirms. The same machinery thus characterises both when recursive reasoning has room to improve at the trajectory level and when the model’s internal guide can recover it.

1. Introduction

While large, compute-intensive models have dominated recent progress on structured reasoning tasks, recursive architectures (Wang et al., 2025; Jolicoeur-Martineau, 2025) have shown breakthrough performance, matching large language models, with neural backbones of as little as $7M$ parameters. This combination of compactness and performance makes them well-positioned for AI deployment in settings with strict latency, privacy, and auditability constraints, where

¹digiLab, UK ²University of Bristol, UK. Correspondence to: Andrew Corbett <andy.corbett@digilab.ai>.

they can offer practical advantages over hyper-scaled alternatives. We argue that what these architectures do at inference time is best understood as approximate inference over latent reasoning trajectories, with deterministic recursion as the one-particle, zero-noise limit.

Prototypical architectures, such as the Tiny Recursive Model (TRM) of Jolicoeur-Martineau (2025), already contain ingredients that suggest a richer inference procedure at test time, including learned early-stopping Q -heads and mixed-frequency latent updates. These features have emerged predominantly through experimental iteration (Wang et al., 2025; Jolicoeur-Martineau, 2025; McGovern, 2025), leaving open how they should be interpreted or used once training is complete. We study this question through inference-time adaptation: given a frozen pre-trained backbone, how should additional computation be allocated across alternative latent reasoning trajectories, and when can we predict that this allocation will succeed?

We make this view operational without retraining. Stochastic perturbations of the inner recursion induce a proposal over neighbouring latent trajectories; the model’s Q -head, repurposed as a learned guide, reweights them online via a Feynman–Kac tilt. The deterministic recursion of Jolicoeur-Martineau (2025) sits inside this framework as the one-particle, zero-noise limit, allowing direct comparison with the original model.

Stochastic exploration substantially increases the number of successful trajectories in the particle cloud, and guided selection identifies them when the guide is aligned. On Sudoku-Extreme (Wang et al., 2025), our method improves exact-solve accuracy from $85.9 \pm 0.6\%$ to $98.0 \pm 0.3\%$, solving previously out-of-reach failure cases and recovering baseline performance at much lower depths (Figure 1).

The procedure helps when two operating conditions are met. Stochastic exploration must be locally stable so alternative trajectories remain recoverable (Proposition 5.1), and the Q -head guide must be aligned with success; that is, able to concentrate particle mass on successful trajectories (Lemma 5.4). Alignment admits both a labelled diagnostic, the class-conditional gap Δ_n , and a label-free necessary condition, the in-cloud guide-spread bound (19), which

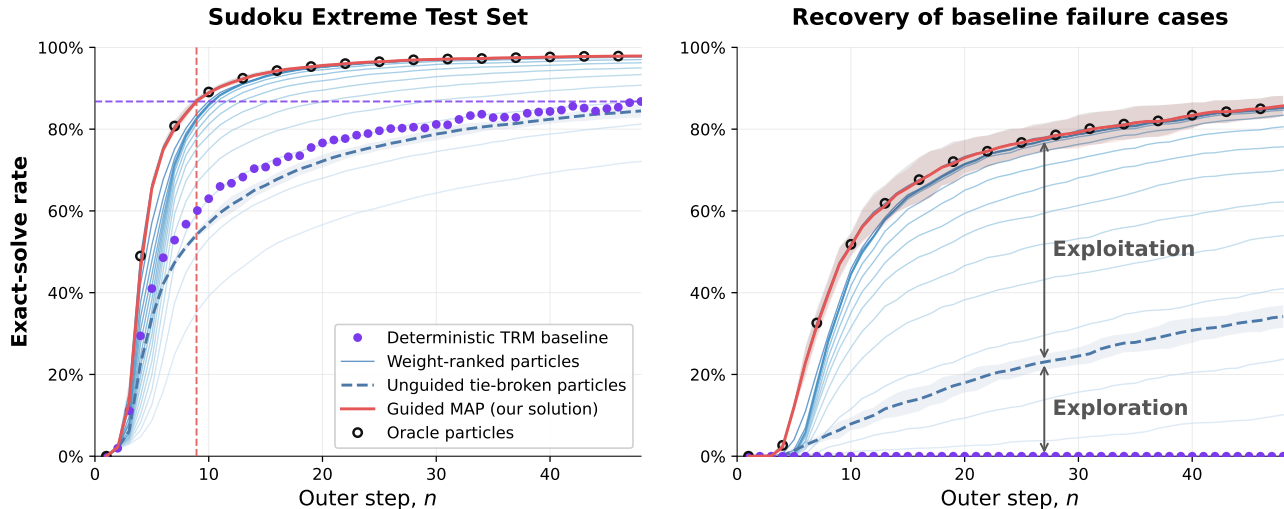


Figure 1. **Inference-time improvement on Sudoku-Extreme.** *Left:* Our method reaches $98.0 \pm 0.3\%$ exact-solve accuracy on the test split, improving over the deterministic TRM baseline ($85.9 \pm 0.6\%$) by step 10. *Right:* On deterministic-failure cases, our method solves $85.9 \pm 1.5\%$ ($35.7 \pm 2.8\%$ unguided; oracle-particle upper bound 86.0%). Results are over $5 \text{ seeds} \times 5 \text{ folds}$; \pm is fold-seed s.d.

upper-bounds the mass shift any tempering can produce. On Sudoku-Extreme both conditions hold, and our method closes nearly the entire oracle gap. On Maze-Hard exploration is stable but the Q -head guide is too flat: the spread bound flags this label-free, a priori (Figure 3), and evaluation confirms the predicted non-improvement (Table 1). The lesson is that recursive models leave useful trajectory-level headroom, but recovering it requires both stable exploration and a ranking-aligned internal guide.

The same probabilistic machinery yields a third diagnostic in the form of uncertainty statistics, addressing output reliability rather than operational regime. Shannon entropies of the final-step and path-integrated token marginals rank token error risk and support selective abstention on both the test split and the harder deterministic-failure split (§5.3, Figure 4).

The remainder develops the method of guided stochastic exploration (§4), the theory and its three diagnostics (§5), and benchmark validation (§6). Our contributions are:

- **An approximate inference framework** for recursive reasoning models: we introduce (i) a stochastic proposal kernel for inference-time exploration and (ii) a guided selection algorithm to identify successful trajectories and reweight the distribution; deterministic recursion is recovered exactly in the one-particle, zero-noise limit with the Q -head guide.
- **Three computable diagnostics** to audit performance and reliability: a stability bound (Proposition 5.1), an alignment characterisation (Lemma 5.4), and uncertainty statistics (§5.3).

- **Zero-retrain exact-solve accuracy improvement** on Sudoku-Extreme, 85.9% to 98.0% . On Maze-Hard, the diagnostic case study correctly predicts, without needing labels, that the learned guide is too flat to exploit the available oracle-particle headroom.

2. Related work

Both the HRM and TRM algorithms (Wang et al., 2025; Jolicoeur-Martineau, 2025) extend earlier recurrent relational networks for constraint-satisfaction puzzles (Palm et al., 2018), showing that strong structured reasoning emerges from repeatedly applying a small recurrent core. Efstathiou & Balwani (2026b) characterise TRM’s recursion as ‘searching’ in an attractor landscape, observing that on Sudoku-Extreme correct solutions sit within reach of the deterministic path: “it’s in there somewhere” (Efstathiou & Balwani, 2026a). We add a probabilistic description in which the Q -head finds them. On Maze-Hard, where no other line of work reports gains, our Q -spread diagnostic identifies the cause label-free while exposing 5% of oracle-particle headroom in the cloud: “it’s in there, too”. Dillon (2026) pursue the orthogonal training-time direction with Adaptive Computation Time (Graves, 2016); ours is a test-time procedure on fixed weights, and the two should compose.

TRM-adjacent work either modifies the model or its training: McGovern (2025) update TRM weights at test time with a self-supervised loss; Asadulaev et al. (2025) reinterpret the inner step as policy improvement and modify it; Abubacar et al. (2026) freeze the backbone and read out a learned quality estimator; Roye-Azar et al. (2025) im-

pose inductive biases for harder generalisation. Looped and latent-compute language models extend recursion depth at inference (Koishekenov et al., 2025; Zhu et al., 2025; Bae et al., 2025). Our setting is complementary on each of these axes: weights, latent depth, and outputs are all unchanged; we only reallocate compute across stochastic local trajectories around the deterministic path and reweight them with the existing Q -head.

At a higher level, the work sits alongside inference-time-compute methods for language models that sample chains, branch search, or apply verifiers (Wei et al., 2022; Wang et al., 2023; Yao et al., 2023; Lightman et al., 2024; Snell et al., 2025). We run the same probabilistic machinery (sequential Monte Carlo with a learned twist) but over continuous latent reasoning states inside a small recursive model, rather than over discrete token chains where the analogous twist function appears in twisted SMC (Zhao et al., 2024). The proposal–twist–resampling pipeline is the same, only the objects being weighted differ. Recursive computation also relates to Deep Equilibrium Models (Bai et al., 2019) and unrolled policy iteration (Behzadian et al., 2026).

Methodologically, we draw on sequential importance sampling and the Feynman–Kac view of weighted path measures (Liu, 2001; Gilks & Berzuini, 2001; Del Moral et al., 2006); the Q -head reweighting is a generalised-Bayes tilt (Bissiri et al., 2016). Our cloud-uncertainty statistics relate to entropy-based uncertainty diagnostics for language models (Kuhn et al., 2023; Farquhar et al., 2024).

3. Background on recursive models

TRM-style architectures (Wang et al., 2025; Jolicoeur-Martineau, 2025) apply a shared backbone f_θ in two nested loops. An inner loop refines a latent state $z \in \mathcal{Z}$ and an outer loop reads out an answer $y \in \mathcal{Y}$, both in $\mathcal{Y} = \mathcal{Z} := \mathbb{R}^{L \times D}$ (L sequence length, D feature dimension). We pair them as the joint state $h_n := (y_n, z_n) \in \mathcal{H} := \mathcal{Y} \times \mathcal{Z}$ at outer step n . In this work we consider the backbone parameters θ fixed, and f_θ as a pre-trained deterministic function. For a fixed embedded input $x \in \mathbb{R}^{L \times D}$, the inner recursion, for $m = 1, \dots, M$, is given by the recursive formula

$$\begin{aligned} z_{n,1} &= f_\theta(x + y_n + z_n), \\ z_{n,m+1} &= f_\theta(x + y_n + z_{n,m}), \end{aligned} \quad (1)$$

and the outer step, through (1), reads out the next answer from the final inner latent step $z_{n,M}$:

$$h_n = (y_n, z_n) \mapsto (f_\theta(y_n + z_{n,M}), z_{n,M}), \quad (2)$$

Iterating (1)–(2) from a learned initial state $h_0 = (y_0, z_0)$ produces a deterministic trajectory h_0, h_1, \dots, h_N , with decoded answers $a_n := \text{Decode}(y_n)$ at each outer step $n = 1, \dots, N$.

An early-stopping utility. The architecture additionally carries a learned scalar Q -head $\tilde{q}_\theta : \mathcal{Y} \rightarrow \mathbb{R}$, trained under detached BCE supervision as a binary classifier for whether a_n matches the ground-truth solution. Jolicoeur-Martineau (2025) use it to trigger Adaptive Computation Time (Graves, 2016). We read this as the model’s internal logit-scale estimate of halting success, and §4 uses it as the natural score on which to tilt the predictive law.

Notation. We identify tensors in $\mathbb{R}^{L \times D}$ with their vectorisations in \mathbb{R}^{LD} and write $\|\cdot\|$ for the induced Euclidean / Frobenius norm; the same symbol is used throughout §4–§5. For isotropic Gaussian noise $\xi_m \sim \mathcal{N}(0, I_{LD})$ the second-moment bound in Proposition 5.1 satisfies $\nu^2 = \mathbb{E}\|\xi_m\|^2 = LD$. We write $\text{sigmoid}(y) := (1 + e^{-y})^{-1}$ for the sigmoid link function.

4. Guided Stochastic Exploration

We build on the deterministic recursion of §3 to construct a path measure over latent reasoning trajectories: a stochastic kernel, generalising the inner-recursion (1), proposes neighbouring trajectories (§4.1); the Q -head reweighting tilts the predictive law toward correct solutions (§4.2); and a bootstrap particle approximation makes the resulting Feynman–Kac flow tractable (§4.3).

4.1. Exploration: the stochastic proposal

To widen the inner TRM recursion for exploration, let $\xi_{n,0:M}$ be independent mean-zero noise variables and $\sigma \geq 0$ the exploration scale. Define

$$\begin{aligned} \zeta_{n,1} &= z_{n,1} + \sigma \xi_{n,0}, \\ \zeta_{n,m+1} &= f_\theta(x + y_n + \zeta_{n,m}) + \sigma \xi_{n,m}, \end{aligned} \quad (3)$$

for $m = 1, \dots, M - 1$, and the stochastic outer update

$$h_n = (y_n, z_n) \mapsto (f_\theta(y_n + \zeta_{n,M}) + \sigma \xi_{n,M}, \zeta_{n,M}). \quad (4)$$

The proposal kernel is then the distribution induced by this random transition:

$$\begin{aligned} K_{f_\theta, x}(A | h_n) &:= \\ &\mathbb{P}((f_\theta(y_n + \zeta_{n,M}) + \sigma \xi_{n,M}, \zeta_{n,M}) \in A), \end{aligned} \quad (5)$$

for measurable $A \subseteq \mathcal{H}$, with implicit dependence on the inner depth M and noise scale σ through (3). At $\sigma = 0$ the kernel collapses to the Dirac measure on (2), recovering the deterministic TRM update. For $\sigma > 0$ it widens the inner trajectory locally without changing backbone weights.

4.2. Exploitation: the Q -head tilt

Local exploration alone defines the proposal kernel (5); we select among proposals by reweighting with the Q -head \tilde{q}_θ ,

instantiated as a Feynman–Kac tilt (Del Moral et al., 2006) of the predictive law.

Let π_n denote the law of the guided state after n outer steps. Propagation through the proposal kernel gives the predictive law

$$\pi_{n+1|n}(dh') = \int_{\mathcal{H}} K_{f_{\theta},x}(dh' | h) \pi_n(dh), \quad (6)$$

which we tilt by the Q -head. Working on the log-probability scale,

$$q_{\theta}(h) := \log \text{sigmoid}(\tilde{q}_{\theta}(y)), \quad (7)$$

where $h = (y, z)$, so that $G_{\beta}(h) := \exp(\beta q_{\theta}(h)) \in (0, 1]$ is a proper potential for every inverse temperature $\beta \geq 0$. The guided update is the exponentially tilted β -law

$$\pi_{n+1,\beta}(dh) \propto G_{\beta}(h) \pi_{n+1|n}(dh), \quad (8)$$

a single mutation–selection step of the corresponding Feynman–Kac flow.

4.3. Finite-particle implementation

We approximate (6) by an empirical measure $\pi_n(dh) \approx \sum_{s=1}^S w_n^{(s)} \delta_{h_n^{(s)}}(dh)$. Propagating each particle through the proposal kernel gives the predictive mixture

$$\pi_{n+1|n}(h) \approx \sum_{s=1}^S w_n^{(s)} K_{f_{\theta},x}(h | h_n^{(s)}), \quad (9)$$

and the update therefore decomposes into exploration (§4.1) and guide-based exploitation (8),

$$\text{Exploration: } h_{n+1}^{(s)} \sim K_{f_{\theta},x}(\cdot | h_n^{(s)}), \quad (10)$$

$$\text{Exploitation: } w_{n+1}^{(s)} \propto w_n^{(s)} G_{\beta}(h_{n+1}^{(s)}). \quad (11)$$

Algorithm 1 gives the bootstrap particle approximation (9). TRAJECTORYSAMPLER stochastically generalises the inner TRM recursion (1)–(2); the outer Q -tempered particle filter generalises single-path rollout to a weighted cloud, with deterministic TRM as the zero-noise, single-particle path. Resampling triggers only when the effective sample size

$$\text{ESS}_n := \left(\sum_s (w_n^{(s)})^2 \right)^{-1} \quad (12)$$

falls below $\tau_{\text{ESS}} S$, using the systematic protocol (Gilks & Berzuini, 2001): ancestor indices $a_{1:S}$ are drawn from the cumulative-weight CDF at stratified levels with a single shared uniform offset, replicating high-weight particles and dropping low-weight ones at the uniform new weight $1/S$. The terminal decoder returns the weighted MAP over decoded answers.

Remark 4.1 (Parallelisation and the deterministic limit). The per-particle steps in Algorithm 1 are independent across s , so parallel execution matches the 1-particle wall-clock. With $S = 1$ and $\sigma = 0$, the algorithm reduces exactly to the deterministic TRM (Jolicoeur-Martineau, 2025).

Algorithm 1 Guided stochastic exploration. Hyperparameters: S particles, outer depth N , inner depth M , noise $\sigma \geq 0$, inverse temperature $\beta \geq 0$, threshold $\tau_{\text{ESS}} \in (0, 1]$.

Require: input x , initial state h_0 , backbone f_{θ} , guide q_{θ}
 1: **function** TRAJECTORYSAMPLER($h = (y, z)$)
 2: draw $\xi_{0:M} \sim \mathcal{N}(0, I_{LD})$
 3: $\zeta_1 \leftarrow f_{\theta}(x + y + z) + \sigma \xi_0$
 4: **for** $m = 1, \dots, M - 1$ **do**
 5: $\zeta_{m+1} \leftarrow f_{\theta}(x + y + \zeta_m) + \sigma \xi_m$
 6: **end for**
 7: **return** ($f_{\theta}(y + \zeta_M) + \sigma \xi_M, \zeta_M$)
 8: **end function**

Outer loop: q_{θ} -tempered particle filter

9: Initialise $h_0^{(s)} = h_0, w_0^{(s)} = 1/S$ for $s = 1, \dots, S$
 10: **for** $n = 0, \dots, N - 1$ **do**
 11: **for** $s = 1, \dots, S$ **do**
 12: $h_{n+1}^{(s)} \leftarrow \text{TRAJECTORYSAMPLER}(h_n^{(s)})$
 13: $\tilde{w}_{n+1}^{(s)} \leftarrow w_n^{(s)} \exp(\beta q_{\theta}(h_{n+1}^{(s)}))$
 14: **end for**
 15: $w_{n+1}^{(s)} \leftarrow \tilde{w}_{n+1}^{(s)} / \sum_r \tilde{w}_{n+1}^{(r)} \forall s = 1, \dots, S$
 16: **if** $\text{ESS}_{n+1}/S < \tau_{\text{ESS}}$ **then**
 17: $h_{n+1}^{(s)} \leftarrow h_{n+1}^{(a_s)}, w_{n+1}^{(s)} \leftarrow 1/S$
 18: **end if**
 19: **end for**
 20: **return** $\hat{a}_N(x) \in \arg \max_a \sum_{s: \text{Decode}(y_N^{(s)})=a} w_N^{(s)}$

5. Operating theory and diagnostics

The probabilistic formulation in §4 lets us characterise when the Q -head’s re-ranking is aligned with successful trajectories. The theory yields two conditions for whether guided exploration helps, *tube stability* (§5.1) and *guide alignment* (§5.2), plus a third, output-side diagnostic, *token-marginal entropy* (§5.3), on the resulting particle cloud.

5.1. Local tube stability of stochastic trajectories

We analyse the local properties of the inner recursion (3). The resulting predictions are measured in Figure 2.

Fix $x \in \mathbb{R}^{L \times D}$ and $h_n \in \mathcal{H}$, and suppress these, as well as subscripts n , from the notation. Let $z_{1:M}$ denote the deterministic inner trajectory and $\zeta_{1:M}$ the stochastic rollout of (3). Write $e_m := \zeta_m - z_m$ and

$$\tau_r := \inf\{m \in \{1, \dots, M\} : \|e_m\| > r\} \quad (13)$$

for the deviation at step m and the first-exit step from the r -tube around the deterministic path, respectively, with the convention $\tau_r = M + 1$ when the set is empty.

Proposition 5.1 (Tube stability). *Assume there exist $r > 0$ and $\rho_r \in [0, 1]$ such that $z \mapsto f_{\theta}(x + y_n + z)$ is ρ_r -Lipschitz on the r -tube $\bigcup_{m=1}^M \{z : \|z - z_m\| \leq r\}$, and that the noise variables are independent, mean-zero, with $\mathbb{E}\|\xi_m\|^2 \leq \nu^2$. Then for $m = 1, \dots, M$ the average in-tube deviations*

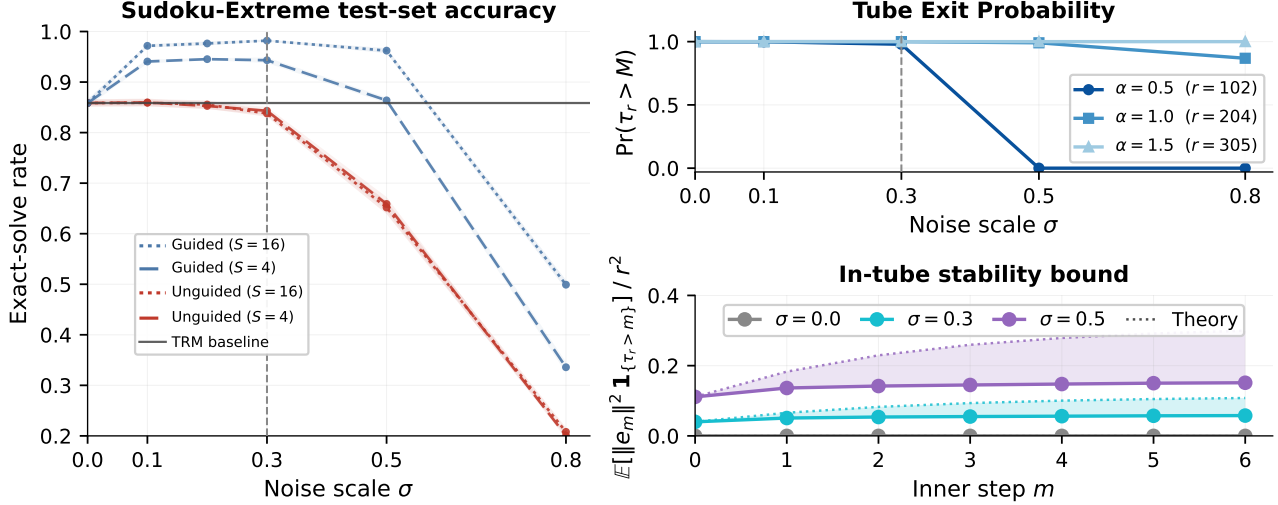


Figure 2. **Local stability and the noise sweet spot on Sudoku-Extreme.** *Left:* terminal exact-solve rate vs. σ for unguided ($\beta = 0$) and guided ($\beta = 0.25$) inference at $S \in \{4, 16\}$. *Right, top:* tube-survival probability $\Pr(\tau_r > M)$ vs. noise scale for radii $r = \alpha\sqrt{LD}$. *Right, bottom:* average in-tube deviations $\mathbb{E}[\|e_m\|^2 \mathbf{1}_{\{\tau_r > m\}}] / r^2$ per inner step at $\alpha = 1.5$; dotted curves give the bound (14) at $\hat{\rho}_r$, the empirical local Lipschitz constant on the r -tube estimated as the maximum secant ratio over 16 random unit-direction probes at each point z_m , $0 \leq m \leq M$. At $\sigma = 0.3$, accuracy is maximised and tube-containment remains high, with deviations within the theory bound.

conform to the geometric decay bound

$$\mathbb{E}[\|e_m\|^2 \mathbf{1}_{\{\tau_r > m\}}] \leq \sigma^2 \nu^2 \sum_{j=0}^{m-1} \rho_r^{2j} \leq \frac{\sigma^2 \nu^2}{1 - \rho_r^2}. \quad (14)$$

Corollary 5.2 (Finite-horizon tube-exit probability). *Under the hypotheses of Proposition 5.1 we have*

$$\mathbb{P}(\tau_r \leq M) \leq \frac{M}{r^2} \frac{\sigma^2 \nu^2}{1 - \rho_r^2}. \quad (15)$$

Proposition 5.1 controls the deviation e_m while the rollout stays in the r -tube; Corollary 5.2 then quantifies how often that control applies. Together (14)–(15) identify the regime in which stochastic widening remains controlled. Fixed M , larger r , smaller σ , and stronger local contraction all tighten both bounds. We evaluate these bounds empirically in Figure 2, showing that the deviation bound is not exceeded and that the probability of remaining within the tube is high at moderate noise levels.

Remark 5.3. Viewed as the unit-step Euler–Maruyama discretisation of a formal diffusion (Song et al., 2021), these are the discrete-time analogues of the familiar $O(\sigma^2)$ variance control for a locally contractive SDE; we do not pursue the continuum limit given the short rollout depth $M \leq 6$.

5.2. Alignment of the Q -head guide

Here we show that the BCE-trained Q -head is aligned with its training label in the integrated-covariance sense of (16) below. The family $\{\pi_{n+1,t}\}_{t \in [0,\beta]}$ in (8) is a one-parameter

exponential tilt, such that bounded $\varphi : \mathcal{H} \rightarrow \mathbb{R}$ satisfies the tilt-derivative identity (Del Moral et al., 2006)

$$\frac{d}{dt} \mathbb{E}_{\pi_{n+1,t}}[\varphi(h)] = \text{Cov}_{\pi_{n+1,t}}(\varphi(h), q_\theta(h)). \quad (16)$$

We call a guide q_θ aligned with φ on $[0, \beta]$ if and only if $\text{Cov}_{\pi_{n+1,t}}(\varphi, q_\theta) \geq 0$ throughout. Equivalently, $\mathbb{E}_{\pi_{n+1,t}}[\varphi(h)]$ is non-decreasing in t on the tilting path $[0, \beta]$. Integrating yields an improvement measure against an ‘unguided’ baseline.

Lemma 5.4 (BCE alignment). *Let $Y \in \{0, 1\}$ and let $0 < \eta < 1$ be a random variable with $\mathbb{E}[Y | \eta] = \eta$. For any strictly increasing ψ , the guide $q_\theta = \psi(\eta)$ satisfies*

$$\text{Cov}_{\pi_{n+1,t}}(Y, q_\theta) \geq 0 \quad \text{for all } t \in [0, \beta].$$

In particular, for $q_\theta = \log \eta$, the population BCE optimum among guides on which η is the conditional expectation of Y , is aligned with Y .

TRM’s Q -head is trained under BCE, so Lemma 5.4 applies with $\eta = \text{sigmoid}(\tilde{q}_\theta(y))$. While Lemma 5.4 establishes alignment in principle (cf. Appendix G.1), in practice we want to test it from inference traces, both with labels (post-hoc) and label-free. For $H \sim \pi_{n+1,t}$, write

$$p_n(t) := \mathbb{P}_{\pi_{n+1,t}}(H \in A_n) \quad (17)$$

for the probability mass on the success set $A_n \subseteq \mathcal{H}$ under the tilted law. We then introduce two scalar quantities derived from (16) that test alignment at outer step n (Figure 3).

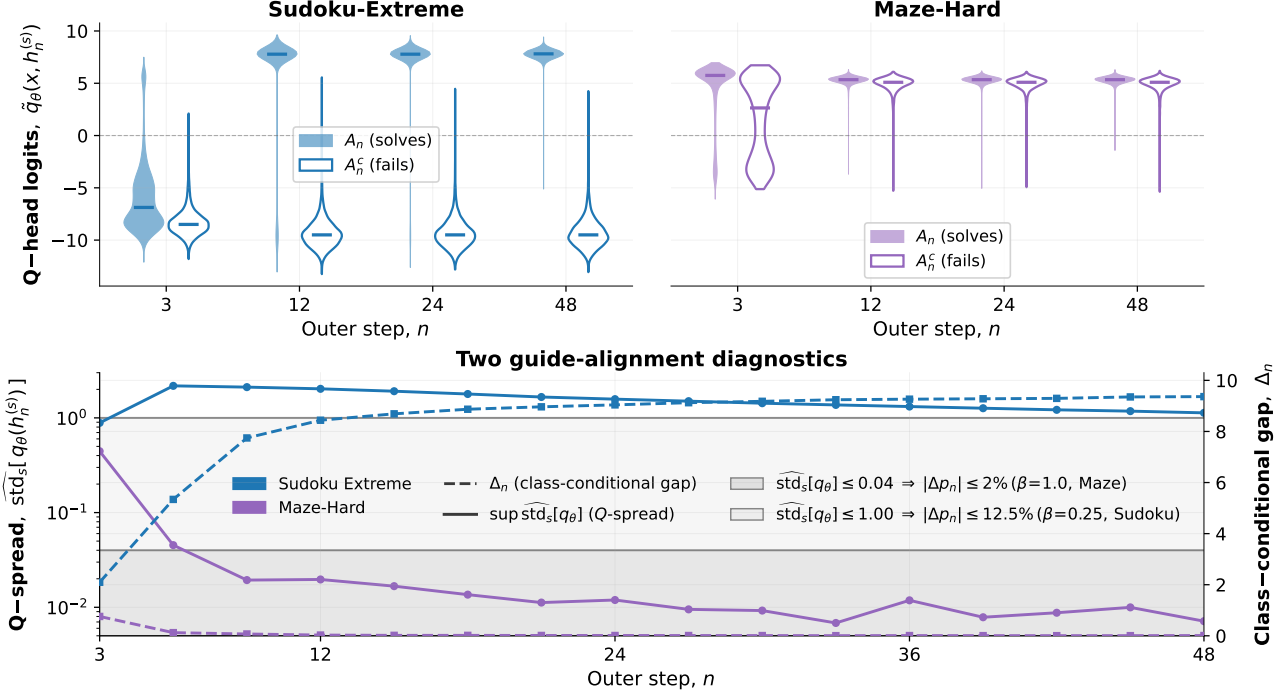


Figure 3. **Guide-alignment diagnostics.** Top: shows \tilde{q}_θ logits split by puzzle-solve outcome over outer step n ; strong class separation on Sudoku-Extreme (left), failure to discriminate on Maze-Hard (right). Bottom: the post-hoc class-conditional gap $\hat{\Delta}_n$ (18) (right-axis, dotted) and the Q -spread bound (19) (left-axis, solid) for the mass shift $|p_n(\beta) - p_n(0)|$. On Maze-Hard the bound is prohibitive: $\leq 2\%$ at $\beta = 1$, tightening to $\leq 0.5\%$ at $\beta = 0.25$; on Sudoku-Extreme the bound exceeds 12.5% at $\beta = 0.25$, in line with the observed improvement (Figure 1).

Class-conditional gap. Here we define a post-hoc diagnostic to measure (16) in the binary-outcome case; see Appendix F for derivation and discussion. For $\varphi = \mathbf{1}_{A_n}$, the covariance (16) factorises as $p_n(t)(1 - p_n(t)) \Delta_n(t)$ with

$$\Delta_n(t) := \mathbb{E}_{\pi_{n+1,t}}[q_\theta | A_n] - \mathbb{E}_{\pi_{n+1,t}}[q_\theta | A_n^c]. \quad (18)$$

Alignment on $[0, \beta]$ is therefore equivalent to the scalar condition $\Delta_n(t) \geq 0$ for all $t \in [0, \beta]$. The sample diagnostic $\hat{\Delta}_n$ requires success labels and is therefore a post-hoc score. Figure 3 tracks (18) directly on saved particle clouds and shows the predicted mass shift emerging as soon as the Q -head separates successful from unsuccessful trajectories. Intuitively, $\hat{\Delta}_n$ is the gap between the mean Q -head logit on solving particles and on failing ones. It accounts for the ‘space’ the guide has to discriminate.

Guide spread over the cloud. A label-free necessary condition for a non-trivial tempering improvement can be observed in the cloud directly. Applying Cauchy–Schwarz to (16) with $\text{std}(\mathbf{1}_{A_n}) \leq \frac{1}{2}$ yields the integrated bound

$$|p_n(\beta) - p_n(0)| \leq \frac{\beta}{2} \sup_{t \in [0, \beta]} \widehat{\text{std}}_s[q_\theta(h_n^{(s)})], \quad (19)$$

where $\widehat{\text{std}}_s$ denotes the empirical standard deviation over particles and the supremum is taken over $h_{n+1}^{(s)} \sim \pi_{n+1,t}$.

A non-negligible $\widehat{\text{std}}_s$ is therefore necessary (but not sufficient) for a meaningful tempering improvement at outer step n . Indeed, the spread bounds the rate of mass shift $|p_n(\beta) - p_n(0)|$ in either direction, so a small spread can rule out gains a priori.

In Figure 3 (bottom), the Maze-Hard Q -spread satisfies $\sup_{t \leq \beta} \widehat{\text{std}}_s[q_\theta] \leq 0.04$. By (19), this caps the achievable mass shift $|\Delta p_n|$ at 2% for $\beta = 1$ and 0.5% for $\beta = 0.25$, well below the 5% oracle headroom on Maze-Hard. On Sudoku-Extreme, by contrast, the spread is large enough that (19) permits at least a 12.5% mass shift at $\beta = 0.25$, consistent with the observed improvement (Figure 1).

5.3. Token entropy as an uncertainty diagnostic

Modelling a particle distribution (6) also yields in-cloud uncertainty diagnostics at the token level. Since (16) holds for any bounded $\varphi : \mathcal{H} \rightarrow \mathbb{R}$, token-class marginals are obtained without modification to Algorithm 1. Let $\text{Dec} : \mathcal{H} \rightarrow \{1, \dots, C\}^L$ be the deterministic decoder. For each token-class pair (ℓ, k) , define $\varphi_{\ell,k}(h) := \mathbf{1}\{\text{Dec}(h)_\ell = k\}$ and $p_{\ell,k}(\beta; n) := \mathbb{E}_{\pi_{n+1,\beta}}[\varphi_{\ell,k}]$; this is the one-dimensional Feynman–Kac projection of (6) onto token-class (ℓ, k) , with evolution governed by (16) under tempering.

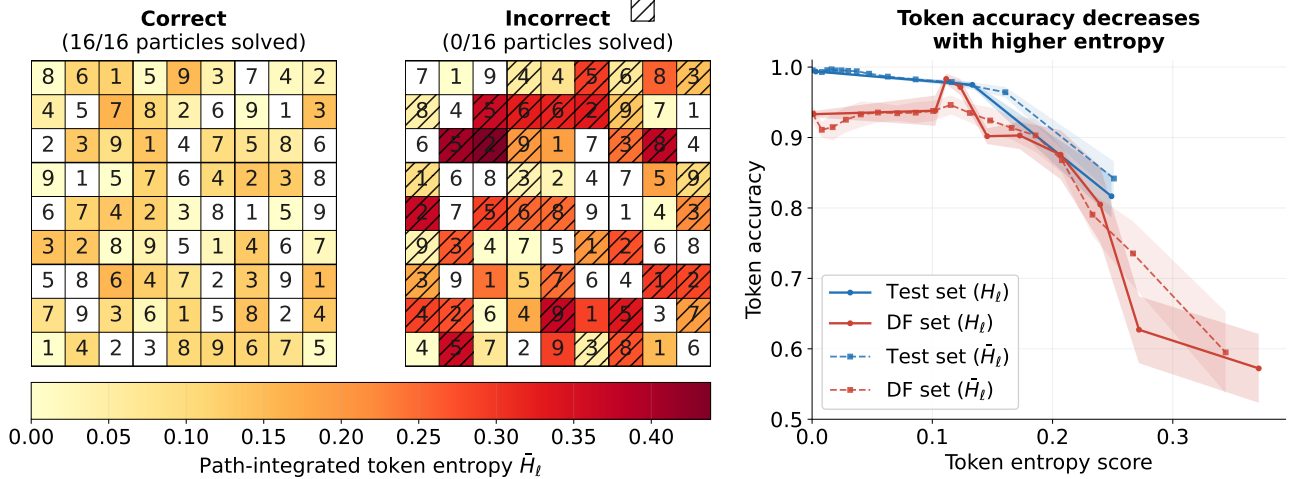


Figure 4. **Token entropy as a risk-ranking diagnostic on Sudoku-Extreme.** *Left, middle:* solved and unsolved test puzzles coloured by per-cell path-integrated entropy \bar{H}_ℓ (shaded: incorrect tokens; white: given cells). *Right:* binned token accuracy vs. uncertainty on Test and DF for H_ℓ and \bar{H}_ℓ ; bands are 95% CIs. Token-level AUROC for H_ℓ : Test 0.834 ± 0.011 , DF 0.710 ± 0.014 .

Writing the marginal for each token ℓ as $p_\ell(\beta; n) := (p_{\ell,1}(\beta; n), \dots, p_{\ell,C}(\beta; n))$, we summarise its dispersion by the normalised Shannon entropy, both at the terminal step and aggregated over outer steps n_1, \dots, n_J :

$$\text{Terminal: } H_\ell := \frac{1}{\log C} H(p_\ell(\beta; N)), \quad (20)$$

$$\text{Aggregated: } \bar{H}_\ell := \frac{1}{J \log C} \sum_{j=1}^J H(p_\ell(\beta; n_j)). \quad (21)$$

We treat H_ℓ and \bar{H}_ℓ as risk-ranking diagnostics over token-level errors; empirical AUROCs and selective-prediction curves are in Figure 4.

6. Experimental evaluation

We evaluate guided stochastic exploration (Algorithm 1) on two fixed TRM models trained on Sudoku-Extreme and Maze-Hard, respectively. Hyperparameters are validation-tuned on Sudoku-Extreme and transferred to Maze-Hard without further tuning, with the diagnostics of §5 acting as a verifier; reported numbers are single-shot test-set evaluations (Appendix A).

The diagnostics of §5 predict, before any evaluation, where the procedure should help. The inner-deviation bound (14)–(15) is conformed to on both benchmarks at moderate noise (Figure 2). The Q -spread bound (19) flags the Maze-Hard Q -head as too flat to produce a non-trivial tempering improvement, while Sudoku-Extreme clears both the Q -spread and class-conditional thresholds (Figure 3). The diagnostics therefore predict improvement on Sudoku-Extreme and non-improvement on Maze-Hard.

Table 1 confirms both predictions. On Sudoku-Extreme,

guided MAP closes nearly the entire oracle gap ($85.9\% \rightarrow 98.0\%$), recovering 86.0% on the deterministic-failure split where the baseline scores zero. On Maze-Hard, stochastic exploration exposes 5% of oracle-particle headroom (90.9% vs. baseline 86.6%), but the misaligned Q -head does not concentrate mass on successful trajectories, so guided MAP returns to baseline (85.3% in both unguided and guided settings). Token-marginal entropy ranks misclassification risk on Sudoku-Extreme (Figure 4): abstaining on the upper-decile H_ℓ raises retained exact-solve rate to $100.0 \pm 0.0\%$ on Test and $99.7 \pm 0.3\%$ on DF.

7. Discussion and broader impact

The original motivation for this work was to explore what an approximate Bayesian interpretation of recursive reasoning (Jolicoeur-Martineau, 2025) might reveal about the elusive mechanics of the architecture. The investigation produced a Feynman–Kac-inspired theory that elevates the Q -head from afterthought to central guide for the selection of latent reasoning trajectories. The same machinery characterises both when recursive reasoning has trajectory-level headroom and when the model’s internal guide can recover it, a thesis we believe extends to recursive reasoning more broadly.

What surprised us was the immediate success of both ingredients on Sudoku-Extreme: modest stochastic exploration produced successful trajectories, and the Q -head correctly weighted particles towards these (Figure 1). Maze-Hard was a step into the unknown as no prior work reports improvements there (cf. McGovern, 2025). Stochastic exploration again exposed oracle-level headroom, but, as the theory predicted, the guide could not identify it. The difference in

Table 1. **Terminal exact-solve rates (%)** at $N = 48$ on held-out splits; ‘Oracle’ is the post-hoc best-performing particle. Guided MAP closes the oracle gap on Sudoku-Extreme; on Maze-Hard the gap remains.

Benchmark	Split	Size	TRM	Unguided	Oracle	Guided MAP
Sudoku-Extreme	Test	10,000	85.9±0.6	84.3±0.7	98.0±0.2	98.0±0.3
Sudoku-Extreme	DF	1,400	0.0	35.7±2.8	86.0±1.5	85.9±1.5
Maze-Hard	Test	1,000	86.6±2.1	85.3±3.0	90.9±2.4	85.3±2.5

character between these two benchmarks comes down to the guide. Improvement is “in there”, but the interesting question is: “how do we build the guide that finds it?”

We therefore propose three directions, each expanding the role of the guide. (i) the guide as a first-class design object to handle structural constraints, custom-training objectives, or multi-guide compositions, rather than just the arbitrary choice of the Q -head; (ii) train-time ramifications of the theory (Appendix E) and the inference-time compute efficiency of the particle-based method, including cross-particle parallelism (Remark 4.1) and scaling beyond the S -sweep of Figure 6; and (iii) broader evaluation across reasoning benchmarks, including graph-based reasoning (Sinha et al., 2019), constraint-based language tasks (Clark et al., 2020; Tafjord et al., 2021), and the more computationally intensive ARC-AGI benchmarks (ARC Prize Foundation, 2025).

More broadly, we propose generalisations of the framework beyond recursive reasoning. In AI safety, steering (Turner et al., 2023; Rimsky et al., 2024) has emerged as a promising approach for online adaptation of foundation-model behaviour. A guided variant of this approach brings a new, explicit mechanism for control. Rather than rotating activation vectors directly, a bespoke guide could identify sampled trajectories aligned with pre-trained constraints.

A natural next question is the transfer-learning capacity of small recursive models. If a guide q_A is used up to step n to produce (y_n, z_n) , can z_n seed another task, or can a second guide q_B redirect the same state towards a related solution? This question is especially natural for graph-based reasoning (Palm et al., 2018; Sinha et al., 2019) and rule-governed language tasks (Clark et al., 2020; Tafjord et al., 2021), where success is determined by consistent relational or logical constraints. If such transfer is possible, small recursive models would be more than compact solvers: they would become an example of a foundational reusable reasoning device, whose capabilities are generalist and, crucially, specialised online with a guide.

References

Abubacar, U., Bauer, R., and Kanojia, D. Parameter-efficient quality estimation via frozen recursive models, 2026. URL <https://arxiv.org/abs/2603.14593>.

Accepted to LowResLM Workshop at EACL 2026.

ARC Prize Foundation. ARC-AGI-2. <https://arcprize.org/arc-agi/2/>, 2025. URL <https://arcprize.org/arc-agi/2/>. Dataset and details; code/data repo: <https://github.com/arcprize/ARC-AGI-2>.

Asadulaev, A., Banerjee, R., Karray, F., and Takac, M. Your latent reasoning is secretly policy improvement operator, 2025.

Bae, S., Kim, Y., Bayat, R., Kim, S., Ha, J., Schuster, T., Fisch, A., Harutyunyan, H., Ji, Z., Courville, A., and Yun, S. Mixture-of-recursions: Learning dynamic recursive depths for adaptive token-level computation. In *Advances in Neural Information Processing Systems (NeurIPS 2025)*, 2025. URL <https://openreview.net/forum?id=QuqsEIVWIG>.

Bai, S., Kolter, J. Z., and Koltun, V. Deep equilibrium models. In *Advances in Neural Information Processing Systems*, 2019.

Behzadian, B., Daley, B., Subbaraj, G., and Nassif, H. Unrolled policy iteration for tiny recursive models. OpenReview, ICLR 2026 Workshop RSI Poster, 2026. URL <https://openreview.net/forum?id=rIzREKws05>.

Bissiri, P. G., Holmes, C. C., and Walker, S. G. A general framework for updating belief distributions. *Journal of the Royal Statistical Society: Series B*, 78(5):1103–1130, 2016.

Clark, P., Tafjord, O., and Richardson, K. Transformers as soft reasoners over language. In Bessiere, C. (ed.), *Proceedings of the Twenty-Ninth International Joint Conference on Artificial Intelligence, IJCAI-20*, pp. 3882–3890. International Joint Conferences on Artificial Intelligence Organization, July 2020. doi: 10.24963/ijcai.2020/537. URL <https://doi.org/10.24963/ijcai.2020/537>. Main track.

Del Moral, P., Doucet, A., and Jasra, A. Sequential Monte Carlo samplers. *Journal of the Royal Statistical Society Series B: Statistical Methodology*, 68(3):411–436, 2006. doi: 10.1111/j.1467-9868.2006.00553.x.

- Dillon, J. Speed is confidence, 2026. URL <https://arxiv.org/abs/2601.19085>.
- Efstathiou, A. and Balwani, A. It’s in there somewhere: Space-time minima and recursive model reasoning dynamics. OpenReview, LIT Workshop @ ICLR 2026, 2026a. URL <https://openreview.net/forum?id=kKps9W1K7n>.
- Efstathiou, A. and Balwani, A. Recursive reasoning as attractor landscape search: Mechanistic dynamics of the tiny recursive model. In *Workshop on Latent & Implicit Thinking – Going Beyond CoT Reasoning*, 2026b. URL <https://openreview.net/forum?id=kKps9W1K7n>.
- Farquhar, S., Kossen, J., Kuhn, L., and Gal, Y. Detecting hallucinations in large language models using semantic entropy. *Nature*, 630(8017):625–630, 2024. doi: 10.1038/s41586-024-07421-0.
- Gilks, W. R. and Berzuini, C. Following a moving target — monte carlo inference for dynamic bayesian models. *Journal of the Royal Statistical Society: Series B*, 63(1): 127–146, 2001.
- Graves, A. Adaptive computation time for recurrent neural networks. *arXiv preprint arXiv:1603.08983*, 2016.
- Jolicoeur-Martineau, A. Less is more: Recursive reasoning with tiny networks. *arXiv preprint arXiv:2510.04871*, 2025. doi: 10.48550/arXiv.2510.04871.
- Koch, O. Olivkoch/nano-trm: An implementation of tiny recursive models (trm). GitHub, 2025. URL <https://github.com/olivkoch/nano-trm>.
- Koishekenov, Y., Lipani, A., and Cancedda, N. Encode, think, decode: Scaling test-time reasoning with recursive latent thoughts. *arXiv preprint arXiv:2510.07358*, 2025. doi: 10.48550/arXiv.2510.07358. URL <https://arxiv.org/abs/2510.07358>.
- Kuhn, L., Gal, Y., and Farquhar, S. Semantic uncertainty: Linguistic invariances for uncertainty estimation in natural language generation. In *International Conference on Learning Representations (ICLR)*, 2023.
- Lightman, H., Kosaraju, V., Burda, Y., Edwards, H., Baker, B., Lee, T., Leike, J., Schulman, J., Sutskever, I., and Cobbe, K. Let’s verify step by step. In *International Conference on Learning Representations*, 2024.
- Liu, J. Sequential importance sampling for estimation of bayesian posterior probabilities. *Statistical Science*, 16(3):322–345, 2001. doi: 10.1214/ss/1043481521.
- McGovern, R. Test-time adaptation of tiny recursive models. *arXiv preprint arXiv:2511.02886*, 2025. doi: 10.48550/arXiv.2511.02886. URL <https://arxiv.org/abs/2511.02886>.
- Palm, R., Paquet, U., and Winther, O. Recurrent relational networks. In *Advances in Neural Information Processing Systems (NeurIPS)*, 2018. URL <https://papers.nips.cc/paper/2018/hash/b9f94c77652c9a76fc8a442748cd54bd-Abstract.html>.
- Rimsky, N., Gabrieli, N., Schulz, J., Tong, M., Hubinger, E., and Turner, A. Steering llama 2 via contrastive activation addition. In *Proceedings of the 62nd Annual Meeting of the Association for Computational Linguistics (Volume 1: Long Papers)*, pp. 15504–15522, Bangkok, Thailand, August 2024. Association for Computational Linguistics. doi: 10.18653/v1/2024.acl-long.828. URL <https://aclanthology.org/2024.acl-long.828/>.
- Roye-Azar, A., Vargas-Naranjo, S., Ghai, D., Balamurugan, N., and Amir, R. Tiny recursive models on arc-agi-1: Inductive biases, identity conditioning, and test-time compute. *arXiv preprint arXiv:2512.11847*, 2025. doi: 10.48550/arXiv.2512.11847. URL <https://arxiv.org/abs/2512.11847>.
- Sinha, K., Sodhani, S., Dong, J., Pineau, J., and Hamilton, W. L. CLUTRR: A diagnostic benchmark for inductive reasoning from text. In *Proceedings of the 2019 Conference on Empirical Methods in Natural Language Processing and the 9th International Joint Conference on Natural Language Processing*, pp. 4506–4515, Hong Kong, China, November 2019. Association for Computational Linguistics. doi: 10.18653/v1/D19-1458. URL <https://aclanthology.org/D19-1458/>.
- Snell, C. V., Lee, J., Xu, K., and Kumar, A. Scaling LLM test-time compute optimally can be more effective than scaling parameters for reasoning. In *The Thirteenth International Conference on Learning Representations*, 2025.
- Song, Y., Sohl-Dickstein, J., Kingma, D. P., Kumar, A., Ermon, S., and Poole, B. Score-based generative modeling through stochastic differential equations. In *International Conference on Learning Representations*, 2021.
- Tafjord, O., Dalvi, B., and Clark, P. ProofWriter: Generating implications, proofs, and abductive statements over natural language. In *Findings of the Association for Computational Linguistics: ACL-IJCNLP 2021*, Online, August 2021. Association for Computational Linguistics. doi: 10.18653/v1/2021.findings-acl.317. URL <https://aclanthology.org/2021.findings-acl.317/>.

- Turner, A. M., Thiergart, L., Leech, G., Udell, D., Vazquez, J. J., Mini, U., and MacDiarmid, M. Steering language models with activation engineering, 2023. URL <https://arxiv.org/abs/2308.10248>.
- Wang, G., Li, J., Sun, Y., Chen, X., Liu, C., Wu, Y., Lu, M., Song, S., and Abbasi Yadkori, Y. Hierarchical reasoning model, 2025. URL <https://arxiv.org/abs/2506.21734>.
- Wang, X., Wei, J., Schuurmans, D., Le, Q. V., Chi, E. H., Narang, S., Chowdhery, A., and Zhou, D. Self-consistency improves chain of thought reasoning in language models. In *International Conference on Learning Representations*, 2023.
- Wei, J., Wang, X., Schuurmans, D., Bosma, M., Ichter, B., Xia, F., Chi, E. H., Le, Q. V., and Zhou, D. Chain-of-thought prompting elicits reasoning in large language models. In *Advances in Neural Information Processing Systems*, volume 35, 2022.
- Yao, S., Yu, D., Zhao, J., Shafran, I., Griffiths, T. L., Cao, Y., and Narasimhan, K. Tree of thoughts: Deliberate problem solving with large language models. In *Advances in Neural Information Processing Systems*, volume 36, 2023.
- Zhao, S., Brekelmans, R., Makhzani, A., and Grosse, R. Probabilistic inference in language models via twisted sequential monte carlo. In *Proceedings of the 41st International Conference on Machine Learning (ICML)*, 2024. URL <https://arxiv.org/abs/2404.17546>.
- Zhu, R.-J., Wang, Z., Hua, K., Zhang, T., Li, Z., Que, H., Wei, B., Wen, Z., Yin, F., Xing, H., Li, L., Shi, J., Ma, K., Li, S., Kergan, T., Smith, A., Qu, X., Hui, M., Wu, B., Min, Q., Huang, H., Zhou, X., Ye, W., Liu, J., Yang, J., Shi, Y., Lin, C., Zhao, E., Cai, T., Zhang, G., Huang, W., Bengio, Y., and Eshraghian, J. Scaling latent reasoning via looped language models. *arXiv preprint arXiv:2510.25741*, 2025. doi: 10.48550/arXiv.2510.25741. URL <https://arxiv.org/abs/2510.25741>.

A. Evaluation protocol

Models and data. We consider two frozen TRM models trained with the Nano-TRM framework (Koch, 2025) on Sudoku-Extreme and Maze-Hard (Wang et al., 2025), using Nano-TRM’s default training hyperparameters. Following Wang et al. (2025), we apply 1,000 shuffling augmentations to Sudoku-Extreme training data and no augmentation to Maze-Hard. The model, dataset, and outer horizon $N = 48$ are held fixed throughout, identical to Jolicoeur-Martineau (2025), so only the inference procedure (§4) varies. Figure 5 (§B) shows the contrasting training trajectories for the two Q -heads.

Splits and statistics. For Sudoku-Extreme, we hold out a 500-puzzle validation subset for hyperparameter selection, disjoint from both the 10,000-puzzle Test split and the 1,400-puzzle deterministic-failure (DF) split (DF puzzles are those on which the deterministic TRM baseline fails). For Maze-Hard, the 1,000-puzzle Test split is too small to subdivide; no validation subset is held out, and hyperparameters are transferred from the Sudoku-Extreme sweep (discussion below). Headline experiments are run over 5 data folds (disjoint partition of Test, each fold 20% of Test; see Table 2) \times 5 random seeds (initialisation of stochastic variables), giving 25 independent runs; reported \pm values are seed-fold standard deviations. Hyperparameter ablations on Sudoku-Extreme (Figure 6) use a 2,000-puzzle subset of Test for compute reasons. All training and inference runs use a single H100 GPU.

Hyperparameter selection. Three hyperparameters are common to both benchmarks: $S = 16$ particles, $N = 48$ outer steps, $\tau_{\text{ESS}} = 0.3$. Only the noise scale σ and inverse temperature β vary by benchmark (Table 2). For Sudoku-Extreme, we sweep $\mathfrak{h} := (\sigma, \beta, S, \tau_{\text{ESS}})$ on the validation subset and select $(\sigma, \beta) = (0.3, 0.25)$; reported Test and DF numbers are then a single-shot evaluation of this configuration. For Maze-Hard, no validation set is available, and we deliberately do not tune on Maze-Hard data: S, N, τ_{ESS} are transferred from the Sudoku-Extreme sweep, $\sigma = 0.5$ follows the architectural prior (Maze-Hard’s normalisation scale is larger than Sudoku-Extreme’s), and $\beta = 1$ is a canonical default for non-trivial tempering, rather than the more conservative $\beta = 0.25$ used for Sudoku-Extreme. The role of Maze-Hard here is to test whether the diagnostics of §5 correctly predict failure on a configuration chosen without Maze-Hard data, which they do without observing ground truth data (Appendix B).

Ablation scope. The hyperparameter sweeps in §C are performed on the held-out Test sets and serve as post-tuning robustness checks for the validated (Sudoku-Extreme) and diagnostic-selected (Maze-Hard) configurations. Consistent with the diagnostic prediction, the Maze-Hard Q -head induces a constant response to β (Figure 6), confirming that no β sweep recovers the headroom.

B. Maze-Hard: further analysis

Figure 5 places the Maze-Hard tube-stability evidence, the analogue of Figure 2 for Sudoku-Extreme, alongside the Q -head training diagnostics for both models. Reading the *left* panel shows that, much like Figure 2, the stochastic trajectories of the Maze-Hard model are stable in the sense of Proposition 5.1 for $\alpha \geq 0.5$ and $\sigma \leq 0.3$; the range of stable σ values conforms to the in-tube stability bound (14). However, the *right* panel shows what we believe is a

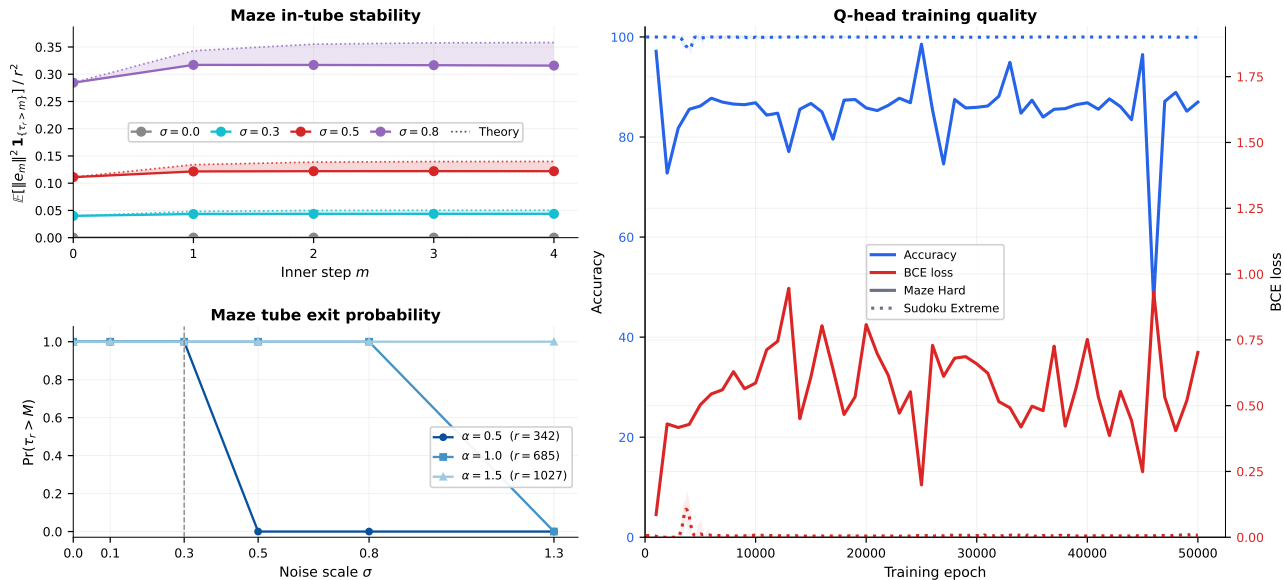


Figure 5. **Maze-Hard case study.** *Top, left:* In-tube deviations $\mathbb{E}[\|e_m\|^2 \mathbf{1}_{\{\tau_r > m\}}] / r^2$ per inner step m at $\alpha = 1.5$, with upper bounds (dotted) from the empirical local-Lipschitz estimate $\hat{\rho}_r$ defined in Figure 2. *Bottom, left:* Tube-survival probability $\Pr(\tau_r > M)$ vs. σ for $r = \alpha\sqrt{LD}$; stable for $\alpha \geq 0.5$, $\sigma \leq 0.3$, matching (14). *Right:* Train-set validation Q -head curves. Sudoku-Extreme saturates near zero BCE and 100% accuracy, while Maze-Hard fails to converge.

Table 2. **Hyperparameters used for main results.** Common across both benchmarks: $S = 16$, $N = 48$, $\tau_{\text{ESS}} = 0.3$. Only σ and β vary by benchmark; selection methodology in ‘Hyperparameter selection’, §A.

Model	σ	β	Splits	Design	Reported as
Sudoku-Extreme	0.3	0.25	Test (10,000), DF (1,400)	5×5 seed-fold	\pm seed-fold s.d.
Maze-Hard	0.5	1	Test (1,000)	5×5 seed-fold	\pm seed-fold s.d.

justification for the poor performance of the in-built guide, observed in Figure 3. We display the training curves for the Q -head on both models, showing extremely high accuracy in the Sudoku-Extreme case, and poor, highly unstable convergence on Maze-Hard. We conjecture this is in part due to the sensitivity of the Maze-Hard structure, in that minor deviations from the solutions lead to poor results, given the objective is to find the ‘shortest’ path to the goal, not just an admissible one; this bimodal objective is not well supported by the BCE objective. A constructive use of the diagnostics for hyperparameter selection (rather than verification) is a natural follow-up; in this paper they serve only as a label-free verifier.

C. Hyperparameter ablation analysis

We report hyperparameter sweeps that complement the headline results of §6; Figure 6 summarises the observations across both benchmarks.

Sudoku-Extreme (top). The β sweep shows that even small amounts of Q -guidance recover the oracle particle,

consistent with the high training-time accuracy of the Q -head (Figure 5, right). Once the oracle is recovered, larger β has no further upside; resampling at high β only distorts the cloud weighting. Terminal accuracy is proportional to the particle count S (middle). This is encouraging for scaling, and motivates us to consider adaptive particle-count schemes as a follow-up.

Maze-Hard (bottom). The sweeps tell quite a clear story: the guide is ineffective at identifying successful trajectories in any regime. The oracle gap is consistently visible, i.e. the cloud contains successful trajectories for every setting, but none of β , S , or τ_{ESS} has any effect on MAP performance. It is noteworthy that the normalised effective sample size holds at $\text{ESS}_n / S \approx 1$ throughout the sweeps (meaning weights stay uniform; no reweighting takes place) so the collapse is a property of the trained Q -head, not of the inference procedure. This makes sense given the near-zero variance in q_θ values (Figure 3, bottom).

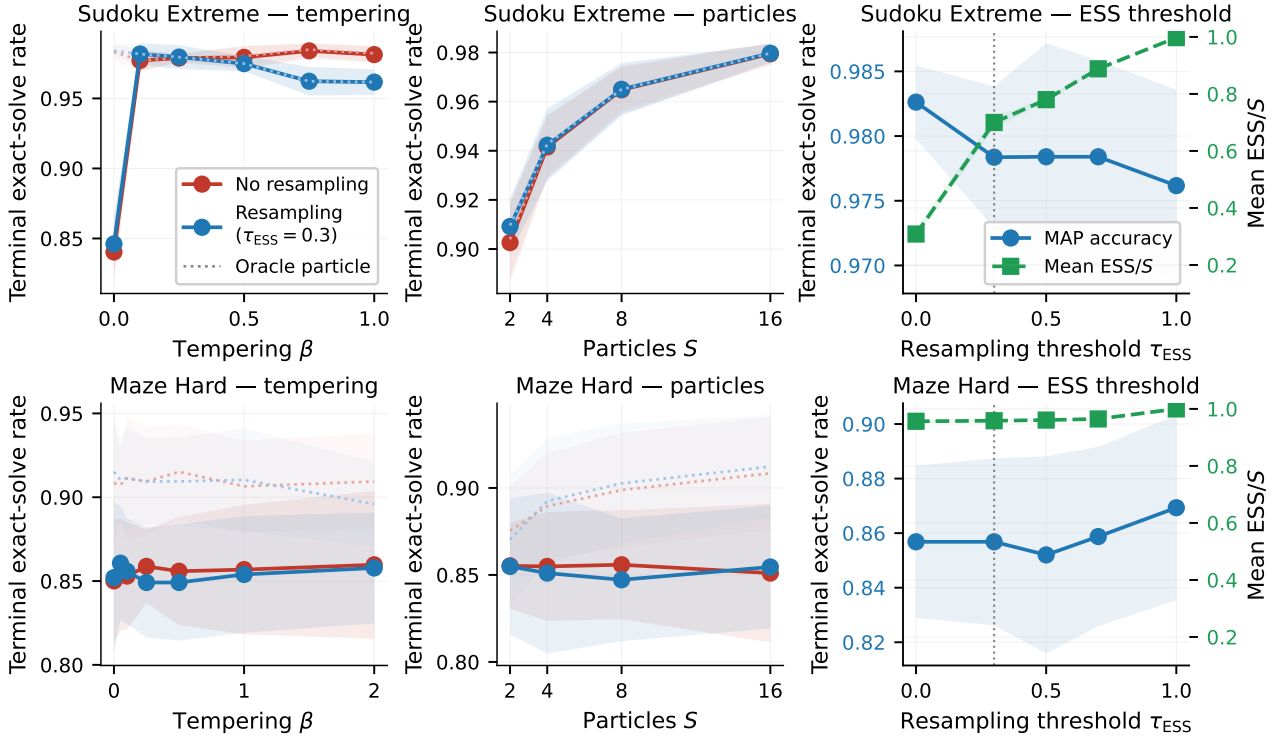


Figure 6. **Hyperparameter sensitivity sweeps.** We report sweeps for Sudoku-Extreme (*top*) and Maze-Hard (*bottom*). *Left*: we vary β across scales, with and without adaptive resampling. *Middle*: we vary the number of particles in the cloud, $S \in \{2, 4, 8, 16\}$. *Right*: we vary the resampling threshold τ_{ESS} . All other hyperparameters are fixed to the values in Table 2.

D. Trajectory contraction in token entropy

To understand the capacity for calibrated uncertainty quantification a little further, we ask the question: ‘how does accumulated entropy measure up against final-prediction entropy?’ The answer, we propose, sheds light on the evolution of uncertainty along the reasoning trajectories.

Specifically, we introduce a blunt measure of the relationship between the two statistics introduced in §5.3: the terminal H_ℓ (20) and the path-integrated \bar{H}_ℓ (21). Define

$$C_\ell := \bar{H}_\ell - H_\ell, \quad (22)$$

the per-token *contraction* between the trajectory mean and the terminal snapshot. Positive C_ℓ therefore implies that the token marginal sharpened towards the final prediction.

Figure 7 reports the per-puzzle average of C_ℓ . The histograms (*left*), separated by solve outcome, reinforce the utility of the diagnostic. Correctly solved puzzles, i.e. every token is correct, admit a clear positive contraction, as expected.

The more remarkable feature is the negative skew of the unsolved-puzzle histogram. With mean contraction near zero, the long left tail represents deepening entropy with the token marginal becoming less concentrated towards the

terminal step. This implies that the trajectories continue to explore rather than settle on a stable incorrect solution.

The scatter plot (*right*) gives a bird’s-eye view of the same data, exposing the magnitudes of \bar{H}_ℓ and H_ℓ rather than only their difference. As expected from Figure 4 (*right*), the highest entropy clusters among unsolved puzzles. More striking is the threshold at roughly (0.1, 0.1): below it, every prediction in the cloud is correct. Could these entropy statistics serve as calibrated guides in their own right?

E. Sudoku-Extreme: train-time efficiency

In this section we ask whether guided stochastic exploration acts as a train-time accelerator: how much earlier in training can it reach the accuracy achieved by the deterministic readout at convergence? Figure 8 applies Algorithm 1 to 19 stored checkpoints from the Sudoku-Extreme training run (epochs 2,499–49,999), under the same five-fold evaluation as the main results; the training loss is shown on the *right*.

The *left* panel reveals two observations. First, guided MAP reaches the deterministic terminal accuracy approximately $3.1\times$ earlier in training than the deterministic readout itself. We take this as a meaningful training-economics signal. Second, the method is stable across the full checkpoint

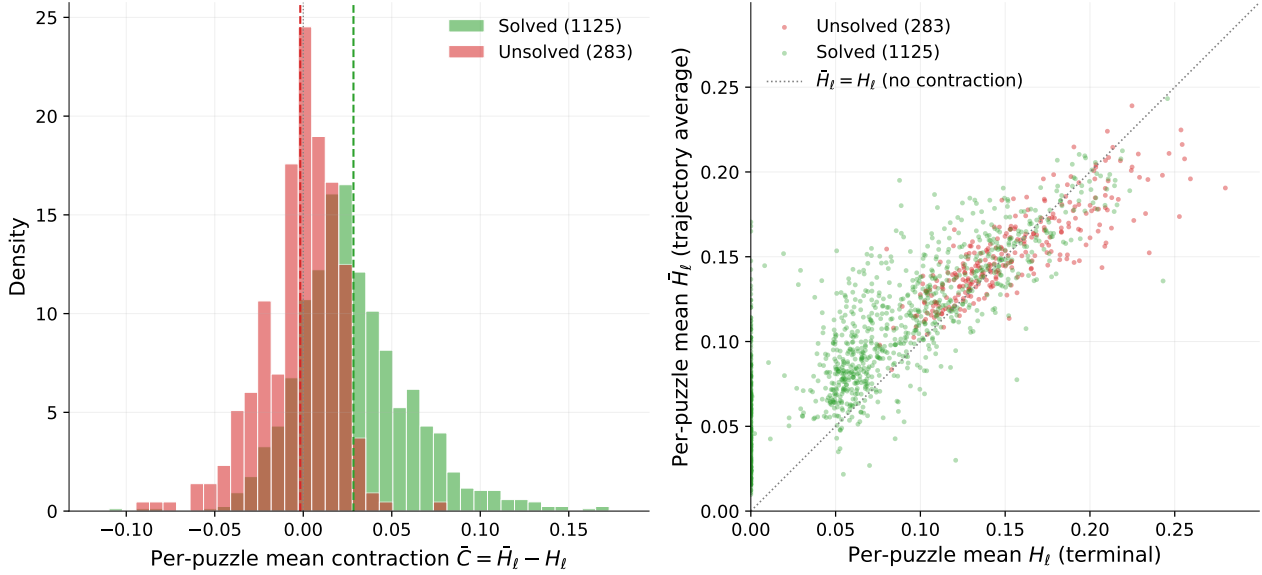


Figure 7. **Trajectory contraction on the deterministic-failure split.** *Left:* histogram of per-puzzle mean contraction $\bar{C} := \text{mean}_\ell C_\ell$ over unmasked tokens, indexed by guided MAP solve outcome. Solved puzzles have mean 0.028 whilst unsolved puzzles have mean -0.002 . *Right:* per-puzzle scatter of trajectory-averaged mean entropy \bar{H}_ℓ against terminal mean entropy H_ℓ , with the identity, $C_\ell = 0$, shown.

range, with no fragility around any particular epoch; this also serves as a secondary ablation on the checkpoint stability of the deterministic TRM core itself.

Remark E.1. The Q -head is far cheaper to train than the TRM backbone: it is a classifier whose loss converges quickly (Figure 5, right), whereas the backbone is the expensive object (Figure 8, right). This asymmetry supports the bespoke-guide direction in §7: a separately trained guide can ride on top of an existing TRM without re-touching the backbone.

F. Analysis of the class-conditional gap

In this section we dig deeper into the guide alignment diagnostic of §5.2. We specialise the Gibbs covariance identity (16) to the binary-success case, yielding a log-odds derivative that directly links the class-conditional gap Δ_n to the mass shift on the success set.

Fix an outer depth n and a measurable success set $A_n \subseteq \mathcal{H}$; in our experiments, A_n is the set of states that solve the puzzle by the terminal horizon N . Write $\varphi := \mathbf{1}_{A_n}$ and $p_n(\beta) := \mathbb{P}_{\pi_{n+1,\beta}}(H \in A_n)$. Applying (16) with $\varphi = \mathbf{1}_{A_n}$ and expanding the covariance gives

$$\begin{aligned} \frac{d}{d\beta} p_n(\beta) &= \text{Cov}_{\pi_{n+1,\beta}}(\mathbf{1}_{A_n}, q_\theta) \\ &= p_n(\beta)(1 - p_n(\beta)) \Delta_n(\beta), \end{aligned} \quad (23)$$

where (cf. (18))

$$\begin{aligned} \Delta_n(\beta) &= \mathbb{E}_{\pi_{n+1,\beta}}[q_\theta(H) \mid H \in A_n] \\ &\quad - \mathbb{E}_{\pi_{n+1,\beta}}[q_\theta(H) \mid H \in A_n^c] \end{aligned} \quad (24)$$

is the class-conditional mean gap in guide score between success and failure states. For $0 < p_n(\beta) < 1$, applying the logit chain rule $\frac{d}{d\beta} \log \frac{p}{1-p} = \frac{1}{p(1-p)} \frac{dp}{d\beta}$ to (23) cancels the variance factor and yields

$$\frac{d}{d\beta} \log \frac{p_n(\beta)}{1 - p_n(\beta)} = \Delta_n(\beta). \quad (25)$$

Equation (25) is the labelled form of the one-number test in §5.2: tempering strictly improves the log-odds of success whenever $\Delta_n(\beta) > 0$, and cannot help when the two classes are indistinguishable under q_θ . The general alignment notion of §5.2 reduces here to $\Delta_n(\beta) \geq 0$ along the tilting path. The binary-success case is the natural setting for future custom guides; for example, classifiers identifying answers that lie outside a pre-trained constraint set (§7), or those that forecast future success (via a delayed training reward).

G. Proofs supporting §5

Here we record the proofs of the theoretical results stated in §5: the BCE-alignment lemma (Lemma 5.4, §5.2) for any strictly increasing transformation, the tube-stability bound (Proposition 5.1, §5.1), and the resulting tube-exit probability (Corollary 5.2).

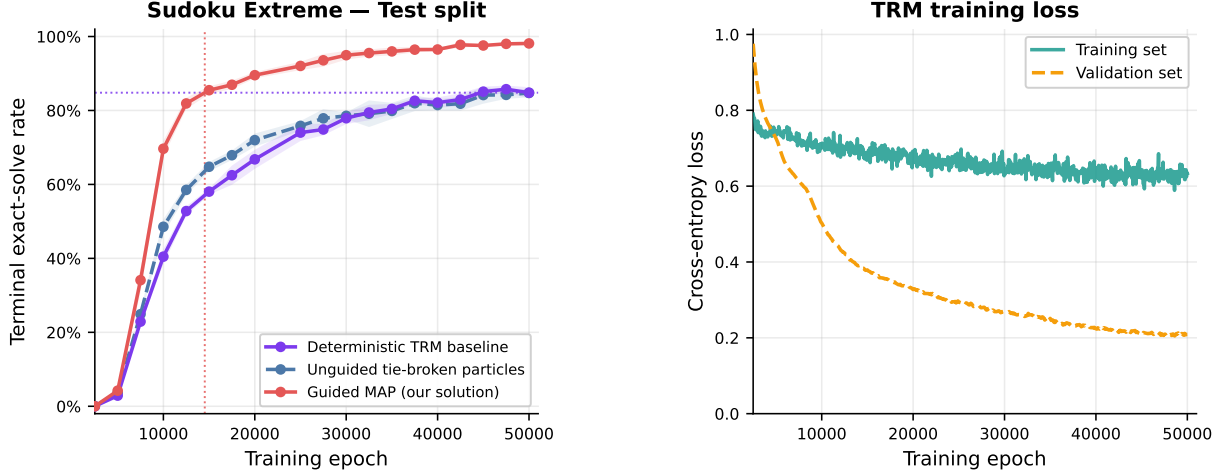


Figure 8. Per-checkpoint scan over the TRM training run. Left: terminal exact-solve rate of guided MAP (red), unguided MAP (blue), and deterministic TRM (purple) across 19 training checkpoints (epochs 2,499–49,999) on the Sudoku-Extreme test split; bands are five-fold standard deviations. Dotted horizontal: deterministic terminal accuracy at epoch 49,999. Dotted vertical: epoch at which guided MAP first crosses this threshold ($\approx 3.1 \times$ earlier than the deterministic readout). Right: TRM training-loss trace (train and validation token cross-entropy) over the same epochs.

G.1. Proof of Lemma 5.4

By the tower property, $\mathbb{E}[Y \mid \eta] = \eta$ gives $\mathbb{E}[Y \psi(\eta)] = \mathbb{E}[\eta \psi(\eta)]$ and $\mathbb{E}[Y] = \mathbb{E}[\eta]$, hence

$$\text{Cov}_{\pi_{n+1,t}}(Y, \psi(\eta)) = \text{Cov}_{\pi_{n+1,t}}(\eta, \psi(\eta)). \quad (26)$$

Strict monotonicity of ψ gives $(\eta - \eta')(\psi(\eta) - \psi(\eta')) \geq 0$ pointwise for an i.i.d. pair (η, η') , and the standard identity $2 \text{Cov}(U, V) = \mathbb{E}[(U - U')(V - V')]$ for i.i.d. copies gives

$$2 \text{Cov}(\eta, \psi(\eta)) = \mathbb{E}[(\eta - \eta')(\psi(\eta) - \psi(\eta'))] \geq 0, \quad (27)$$

with equality iff η is constant on the support of $\pi_{n+1,t}$. The case $\psi = \log$ gives the BCE-population statement. \square

G.2. Proof of Proposition 5.1

Fix $h_n = (y_n, z_n)$ and suppress n, x, h_n from the notation, setting

$$F_\theta(z) := f_\theta(x + y_n + z). \quad (28)$$

Then the deterministic and stochastic inner trajectories satisfy $z_1 := z_{n,1} = f_\theta(x + y_n + z_n)$, $z_{m+1} = F_\theta(z_m)$, as well as $\zeta_1 = z_1 + \sigma\xi_0$, $\zeta_{m+1} = F_\theta(\zeta_m) + \sigma\xi_m$ for $m = 1, \dots, M-1$.

Write $e_m := \zeta_m - z_m$ as in (13), and for $m \geq 0$ let

$$E_m := \{\|e_1\| \leq r, \dots, \|e_m\| \leq r\}, \quad (29)$$

with the convention $E_0 := \Omega$ (the empty intersection); equivalently, $E_m = \{\tau_r > m\}$ for $m \geq 0$.

Base case. Since $e_1 = \sigma\xi_0$ and $\mathbf{1}_{E_1} \leq 1$,

$$\mathbb{E}[\|e_1\|^2 \mathbf{1}_{E_1}] \leq \sigma^2 \mathbb{E}\|\xi_0\|^2 \leq \sigma^2 \nu^2. \quad (30)$$

One-step recursion. Fix $m \in \{1, \dots, M-1\}$, and write

$$D_m := F_\theta(\zeta_m) - F_\theta(z_m), \quad (31)$$

so that $e_{m+1} = D_m + \sigma\xi_m$. Condition on $\mathcal{F}_m := \sigma(\xi_0, \dots, \xi_{m-1})$: both D_m and $\mathbf{1}_{E_m}$ are \mathcal{F}_m -measurable, while $\xi_m \perp \mathcal{F}_m$ has mean zero. Expanding the square and taking expectations, the cross-term vanishes and the noise term satisfies $\mathbb{E}[\|\xi_m\|^2 \mathbf{1}_{E_m}] \leq \mathbb{E}\|\xi_m\|^2 \leq \nu^2$, so

$$\mathbb{E}[\|e_{m+1}\|^2 \mathbf{1}_{E_m}] \leq \mathbb{E}[\|D_m\|^2 \mathbf{1}_{E_m}] + \sigma^2 \nu^2. \quad (32)$$

On E_m , $\|e_m\| \leq r$, so $\zeta_m \in \{z : \|z - z_m\| \leq r\}$; both z_m and ζ_m therefore lie in $\bigcup_{j=1}^M \{z : \|z - z_j\| \leq r\}$, and the local Lipschitz hypothesis gives $\|D_m\| \leq \rho_r \|e_m\|$ on E_m . Substituting into (32) yields the one-step bound

$$\mathbb{E}[\|e_{m+1}\|^2 \mathbf{1}_{E_m}] \leq \rho_r^2 \mathbb{E}[\|e_m\|^2 \mathbf{1}_{E_m}] + \sigma^2 \nu^2. \quad (33)$$

Since $E_{m+1} \subseteq E_m$, in particular

$$\mathbb{E}[\|e_{m+1}\|^2 \mathbf{1}_{E_{m+1}}] \leq \rho_r^2 \mathbb{E}[\|e_m\|^2 \mathbf{1}_{E_m}] + \sigma^2 \nu^2. \quad (34)$$

Iterating the recursion. Define $a_m := \mathbb{E}[\|e_m\|^2 \mathbf{1}_{E_m}]$ for $m = 1, \dots, M$. By (30) and (34),

$$a_1 \leq \sigma^2 \nu^2, \quad a_{m+1} \leq \rho_r^2 a_m + \sigma^2 \nu^2. \quad (35)$$

Iterating gives

$$a_m \leq \sigma^2 \nu^2 \sum_{j=0}^{m-1} \rho_r^{2j} \leq \frac{\sigma^2 \nu^2}{1 - \rho_r^2} \quad (36)$$

for $m = 1, \dots, M$, which recovers (14). \square

G.3. Proof of Corollary 5.2

Using the notation and conventions from the previous proof ($E_m = \{\tau_r > m\}$ for $m \geq 0$, with $E_0 = \Omega$), define

$$b_m := \mathbb{E} [\|e_m\|^2 \mathbf{1}_{E_{m-1}}] \quad (m = 1, \dots, M). \quad (37)$$

We first show that

$$b_m \leq \sigma^2 \nu^2 \sum_{j=0}^{m-1} \rho_r^{2j} \leq \frac{\sigma^2 \nu^2}{1 - \rho_r^2}. \quad (38)$$

For $m = 1$, since $E_0 = \Omega$ and $e_1 = \sigma \xi_0$, $b_1 = \mathbb{E} \|e_1\|^2 \leq \sigma^2 \nu^2$. For $m \geq 1$, the one-step bound (33) gives

$$\begin{aligned} b_{m+1} &= \mathbb{E} [\|e_{m+1}\|^2 \mathbf{1}_{E_m}] \\ &\leq \rho_r^2 \mathbb{E} [\|e_m\|^2 \mathbf{1}_{E_m}] + \sigma^2 \nu^2 \leq \rho_r^2 b_m + \sigma^2 \nu^2, \end{aligned} \quad (39)$$

where the last inequality uses $E_m \subseteq E_{m-1}$ so that $\mathbb{E} [\|e_m\|^2 \mathbf{1}_{E_m}] \leq b_m$. The bound (38) follows by induction.

Next, $\{\tau_r = m\} = E_{m-1} \cap \{\|e_m\| > r\}$, on which $\|e_m\|^2 \mathbf{1}_{E_{m-1}} \geq r^2$. Markov's inequality therefore gives

$$\mathbb{P}(\tau_r = m) \leq \frac{1}{r^2} \mathbb{E} [\|e_m\|^2 \mathbf{1}_{E_{m-1}}] = \frac{b_m}{r^2}. \quad (40)$$

Summing over $m = 1, \dots, M$,

$$\begin{aligned} \mathbb{P}(\tau_r \leq M) &= \sum_{m=1}^M \mathbb{P}(\tau_r = m) \\ &\leq \frac{1}{r^2} \sum_{m=1}^M b_m \leq \frac{M}{r^2} \frac{\sigma^2 \nu^2}{1 - \rho_r^2}, \end{aligned} \quad (41)$$

which recovers (15). \square